Issued: April 1971

LA-4669-MS
UC-80, REACTOR
TECHNOLOGY
TID-4500

LOS ALAMOS SCIENTIFIC LABORATORY
of the
University of California
LOS ALAMOS • NEW MEXICO

Behavior of Sodium-Bonded (U,Pu)C Fuel Elements after Moderate Burnup

by

J. C. Barner

BEHAVIOR OF SODIUM-BONDED (U, Pu)C FUEL ELEMENTS AFTER MODERATE BURNUP

by

J. O. Barner

ABSTRACT

Two sodium-bonded, single phase $(U_{0.8}Pu_{0.2})C$ fueled, Type 316 stainless steel clad fuel elements were irradiated in EBR-II at heating rates of ~30 kW/ft to burnups of 3.7 and 5.0 at.%. No clad failures occurred as a result of the irradiation. Total fission gas release from the fuel was low. Thermal stresses in the fuel resulted in fuel splitting upon initial startup and general fuel fragmentation as fission product recoil and fast neutron damage accumulated. No new phases were observed in the fuel after irradiation.

---

1. INTRODUCTION

The solid solution uranium-plutonium monocarbides are fuel materials of considerable interest for advanced LMFBR application. The interest stems, in part, from the potential of these compounds to operate at high specific powers or high linear heat ratings at relatively low operating temperatures. These attractive operating characteristics are the result of the high thermal conductivity of the monocarbide fuels. The utilization of high conductivity sodium in the fuel-clad annulus allows even lower fuel operating temperatures.

The reference fuel element system being investigated at the Los Alamos Scientific Laboratory is composed of high purity, single phase, solid solution $(U_{0.8}Pu_{0.2})C$ fuel, sodium bonded to thin walled, solution annealed, Type 316 stainless steel cladding. An additional advantage of this system is the superior fuel-clad compatibility resulting from the use of fuel containing no free metal or higher carbides. Results of out-of-pile sodium loop experiments[1] and thermal irradiations[2] have demonstrated that deleterious fuel-clad chemical interactions do not occur between Type 316 stainless steels and single phase $(U_{0.8}Pu_{0.2})C$.

A set of three series of EBR-II irradiation experiments based on this reference fuel element system is currently in progress. A description of the experimental

TABLE I

DESCRIPTION OF EXPERIMENTS

Condition	Series 1	Series 2	Series 3
1. Lineal Power, kw/ft	~ 30	~ 45	~ 30
2. Fuel Composition	——$(U_{0.8}Pu_{0.2})C$, Single-phase, Sintered——		
3. Fuel Uranium	^{235}U	^{233}U	^{235}U
4. Fuel Density	90%	95%	95%
5. Smear Density	80%	80%	80%
6. Clad Size	——0.300-in.-i.d. x 0.010-in. wall——		
7. Clad Type	316 SS	316 SS	316 SS
8. Max Clad Temp. °F (°C)	1250 (677)	1275 (690)	1250 (677)
9. Max Fuel Centerline Temp. °F (°C)*	2130 (1165)	2550 (1399)	2100 (1149)
10. Burnup	——3 at.% to 8 at.%——		

*Calculated for solid fuel pellet.

variables is given in Table I. The notable differences among these three series are the high linear power rating of Series 2 and the higher fuel density of Series 2 and 3.

Two capsules from Series 1, designated 36B and 42B, have been removed from the reactor for examination. Capsule 42B was irradiated in EBR-II subassemblies XO89 and XO70. Capsule 36B was irradiated in subassembly XO70. Both capsules operated at a calculated peak linear heating rate of 29 to 30 kW/ft. The maximum calculated burnups were 3.7 and 5.0 at.% for capsules 36B and 42B, respectively.

This paper deal with the results obtained from the nondestructive examination of capsules 36B and 42B, and the destructive examination of capsule 42B.

II. DESCRIPTION OF THE IRRADIATION EXPERIMENTS

The experimental elements were contained in a standard 40-in. long, 3/8-in. o.d. EBR-II Type A-19 irradiation capsule. The element cladding was fabricated from solution annealed Type 316 stainless steel tubing, 0.300 in. o.d., 0.280 in. i.d., and 36.64 in. long. The element end caps were machined from Type 316 stainless steel sheet, 1/16 in. thick. The fuel was in the form of pressed and sintered right circular cylinders 0.265 in. o.d. and 0.25 in. long. The uranium in the fuel was 93% enriched in ^{235}U. The fuel had a density of 91.0 ± 1.5% of the theoretical density of 13.46 g/cm^3. A detailed description of the synthesis, fabrication and characterization of the fuel can be found in Ref. 3.

The fuel stack consisted of four depleted UC insulator pellets at the bottom, one UC pellet at the top, and 53 fuel pellets between the insulators. The fuel stack was loaded into the elements with a predetermined amount of extruded cold-trapped sodium. The fuel and sodium loading was carried out in a glovebox with an atmosphere of helium containing less than 10 ppm of total water, oxygen, and nitrogen. The resultant contaminant contents in sodium control samples were < 10 ppm carbon, < 1 ppm nitrogen, and 7-16 ppm oxygen. The external surfaces of the element were maintained free of alpha contamination throughout the loading sequence.

Removal from the sodium bond annulus of any fuel chips that might impede fuel swelling during irradiation was accomplished by melting the bonding sodium and centrifuging the sealed element. Wetting of all clad and fuel surfaces by the sodium was accomplished by a heat treatment at 600°C for one hour.

To ensure dependability, several measurements and nondestructive tests were performed on the element components. The fuel was weighed, measured, radiographed, and visually examined. The cladding was fluorescent penetrant tested and ultrasonically examined for defects to a limit of 5% of the wall thickness. All welds were radiographed, fluorescent penetrant tested, and helium leak checked. The assembled element was radiographed, checked for straightness, weighed, and measured; the sodium bond was eddy current tested for defects larger than 0.030 in. in diameter.

A similar procedure was utilized for implementing double encapsulation. A detailed description of the fuel element loading procedure can be found in Ref. 4.

III. EXPERIMENTAL RESULTS

Capsules 36B and 42B were discharged from EBR-II after reactor run 44B at calculated peak burnups of 3.7 and 5.0 at.%, respectively. Neutron radiography

of both capsules was performed at TREAT. Both capsules were then shipped to LASL for complete examination. Nondestructive examinations were done on both capsules and a destructive examination of capsule 42B has been completed.

A. Nondestructive Examination of Capsules 36B and 42B

Capsule 42B was neutron radiographed at 1.5 at.% burnup after irradiation in subassembly XO39. At that time, it was discovered that the upper pellet was fuel rather than UC. This observation was reconfirmed when the elements were neutron radiographed at TREAT after irradiation in XO70. Figure 1 shows a section of the neutron radiograph of capsule 36B. Evidence of axial and transverse cracking of fuel pellets was seen in the radiographs of both capsules. The presence of small fuel chips was observed in both elements on the shelves formed by misaligned UC pellets at the bottom of the fuel stack. Most of these chips were present before irradiation. No evidence for element failure in either experiment was observed in the neutron radiographs.

Radiographs of both capsules were produced at a magnification of ~1.5X using a 22-MeV Betatron x-ray machine. The x-ray radiographs also revealed axial and transverse cracking of fuel pellets in both capsules. Figure 2 shows a section from the radiograph of capsule 36B. The top of a pellet has capped along residual fabrication stresses.

A correlation between the neutron radiographs and x-ray radiographs was made. All 53 fuel pellets in capsule 36B were split at least once axially due to thermal stresses. Fifty-three of the 54 fuel pellets in capsule 42B were cracked. Fifty-two of the 53 cracked pellets were split axially. Transverse cracks and general fragmentation of the fuel pellets were observed in both capsules, particularly in the high temperature, high burnup regions.

All components in both capsules were found to be in their proper positions. No evidence for fuel element failure was observed in the x-ray radiographs of either capsule.

Capsules 42B and 36B were gross gamma scanned over their entire length in 0.015-in. steps with a 0.020-in. collimator. All capsule components were found to be in their proper positions. The fuel stack height in capsule 42B had expanded 2.15%. In the case of capsule 36B, there was a significant activity drop at the top of the capped pellet. Evidence of the fuel chips in the UC insulator regions at the bottoms of the capsules was observed.

Both capsules were also gross gamma scanned over the fueled length in 0.030-in. steps with a 0.004-in. collimator. Examples of this type of scan are shown in Figs. 3 and 4. Figure 3 illustrates a typical region from capsule 42B. The pellet-to-pellet interfaces are easily detected. Figure 4 shows the interface at the capped pellet in capsule 36B. Data of this type were used to determine individual pellet length increases in both capsules. The results are shown in Fig. 5. The fuel movement caused by the capped pellet in capsule 36B is apparent at position 53. The fuel swelling rate for capsule 36B based on the maximum length change, excluding the capped pellet and assuming isotropic swelling, was 2.4 vol% per at.% burnup. The average isotropic swelling rate was 2.0 vol% per at.% burnup. Also shown in Fig. 5 are the individual pellet length changes for capsule 42B. The maximum isotropic swelling rate was 1.2 vol% per at.% burnup. The average isotropic swelling rate was 1.5 vol% per at.% burnup. It is apparent that the damage rate in both capsules is higher in the high fuel temperature, high burnup regions.

Axial multispectral gamma scans of both capsules were also completed. Data was obtained for ^{103}Ru, ^{134}Cs, ^{137}Cs, ^{95}Zr-^{95}Nb, and ^{140}La. All five fission products exhibited nearly identical distributions, indicating that there was no detectable migration of these fission products along the axis of the fuel.

Gamma scanning of the gas plenum regions of both capsules for selected fission products indicated that the fuel elements had not failed.

B. Destructive Examination of Capsule 42B

Prior to the removal of the fuel element from capsule 42B, the outer gas plenum was punctured and a sample taken. No fission gas was found in the sample

as determined using mass spectrographic techniques. Therefore, based on gamma scanning and radiography, the judgment that the inner element had not failed was confirmed.

After the fuel pin from capsule 42B had been removed from the outer clad and thoroughly cleaned, two axial profilometer traces were taken 90° apart at 0° and 270° orientations. The element was then rotated 45° and two more traces were taken at 45° and 315° orientations.

The results of these measurements are shown for the fuel area in Fig. 6. Some fuel-cladding mechanical interaction occurred, resulting in cladding ovality over lengths of up to 2 to 3 in. Very little mechanical interaction on a pellet length pitch (~ 0.250 in.) was observed. The maximum observed deformation was 0.0039 in. or 1.3%. The average deformation in the high fluence region of the element was 0.011 in. or 0.37%. The fast neutron damage linear swelling was calculated using the equations recommended by GE[5] and HEDL[6] for solution annealed Type 316 stainless steel. The GE equation yielded a calculated diameter increase of 0.0023 in. or 0.75%, while the corresponding HEDL value was 0.0007 in. or 0.25%.

The gas plenum of the element was punctured and the gas in the plenum collected. The calculated total gaseous fission product release was 7.7 ± 0.6% of the gas atoms generated, based on the calculated generation rates of Burris and Dillon.[7] A similar calculated release based on the data of Lisman et al.[8] was 6.9 ± 0.6%. The calculated release of individual xenon and krypton is shown in Table II.

Four fueled sections were cut from the element for metallographic examination. The characteristics and irradiation conditions for these sections are described in Table III. Figure 7 illustrates the fuel conditions before irradiation.

The as-polished macrophotograph of the high fuel temperature section 126 (Fig. 8) and the as-polished mosaics of all four sections (Figs. 9, 10, 11, and 12) illustrate the overall mechanical behavior of the fuel. Axial splitting of the pellets due to thermal stresses was evident in all sections. Further fuel

TABLE II

ISOTOPIC FISSION GAS RELEASE

Isotope	Percentage[7] Released	Percentage[8] Released
^{83}Kr	11.6	6.6
^{84}Kr	12.1	6.7
^{85}Kr	6.2	5.8*
^{86}Kr	8.3	6.8
^{131}Xe	6.4	6.4
^{132}Xe	6.7	7.0
^{134}Xe	6.8	7.1
^{136}Xe	6.7	7.0

* Not corrected for decay.

fragmentation was observed with the more severe fracturing occurring in the high burnup, high temperature regions. Fuel clad contact was observed only in section 125, where a misaligned pellet was touching the cladding. No fuel fragments were observed in the fuel-clad annulus.

As-polished radial strips at 100X were prepared for all sections. Figures 13, 14, 15, and 16 illustrate the fuel condition at the fuel temperature extremes in the element. These indicate a general increase of small diameter porosity. In the high temperature, high burnup section, "necklaces" of very small pores, presumably fission gas bubbles, formed in the grain boundaries. These "necklaces" begin to appear at one-half to two-thirds of the distance from the fuel center to the clad in the high temperature sections. These "necklaces" are illustrated at a higher magnification in Fig. 17. The "necklaces" do not appear to a significant degree in the low temperature fuel sections. This general increase in

TABLE III

CHARACTERISTICS AND OPERATING CONDITIONS AT METALLOGRAPHIC SECTIONS

Sample No.	Mean Clad Temp., °C	Heating Rate kw/ft	Burnup at.%	Sample Direction
124	665	25	4.1	Transverse
125	612	30	5.0	Longitudinal
126	604	30	5.0	Transverse
127	515	25	4.2	Transverse

the concentration of small pores, together with dark spots formed by sodium-etchant reaction, causes the high temperature sections to appear darker near the fuel centerline than near the fuel surface.

Photomicrographs of etched fuel were prepared for all sections. Figures 18, 19, 20, and 21 illustrate the fuel condition in radial strips of the four sections. No new phases were observed in the single phase fuel.

Photomicrographs of etched cladding (Figs. 22, 23, and 24) show a slight reaction on the inside surface, presumably due to carburization. The amount of reaction increased with increased cladding operating temperature. The reaction layer penetrated to a depth of approximately 6% of the wall thickness in the high temperature cladding section 124. Grain boundary precipitation of carbides was also observed in the clad sections.

Alpha-autoradiographs of the fuel sections indicated that there was no detectable plutonium redistribution. The alpha-radiographs of the four fueled sections are shown in Figs. 25, 26, 27, and 28.

Beta-gamma-autoradiographs of the fueled sections are shown in Figs. 29, 30, 31, and 32. These show that little fission product migration has occurred in the low fuel burnup, low fuel temperature region. However, in the high burnup, high temperature region of the element, the loss of beta-gamma activity near the centerline of the fuel, adjacent to cracks, and in the areas containing porosity "necklaces" would indicate a significant fission product migration.

Density measurements could not be made due to extensive fuel fragmentation.

A fuel burnup analysis was carried out by Idaho Nuclear Corporation, utilizing the "ASTM Method E-321, Atom Per Cent Fission in Uranium and Plutonium Fuel (^{148}Nd Method)." The results indicated that the peak burnup in capsule 42B was 4.4 at.%.

An attempt was made to determine radial distributions of uranium, plutonium, and fission products in the fuel sections utilizing a shielded microprobe. These measurements were deleteriously affected by the presence of a brownish stain, presumably due to a sodium reaction product which appeared in the fuel between the outer edge and one-half the fuel radius. Uranium and plutonium x-ray intensities in this region were markedly irregular and lower when compared to the central section of the fuel. The presence of sodium in the stained area and its absence in the unstained area were confirmed by microprobe analysis.

The sodium-free regions yielded higher and relatively constant x-ray intensities for uranium and plutonium. It is probable that the x-ray intensities in the stained region are erroneously low due to the absorption of the electron beam by the stain.

Similar difficulties were encountered in the determination of Nd, Ce, Cs, Ru, Mo, Zr, Xe, and I. However, it is notable that Cs and I, which have low boiling points, were both detected in the fuel.

The cladding of the three transverse metallographic sections was examined using the microprobe. Both the low burnup sections 124 and 127 exhibited similar behavior even though these two sections represent the extremes in operating temperatures. For most of the inside diameter of the cladding, no indication of nickel, iron, or chromium depletion was observed. In a very few places, a limited depletion of iron and nickel was found, accompanied by a buildup of chromium. The iron and nickel from the depleted region appear to have moved toward the clad inner surface to produce a thin layer 3 to 5 microns thick.

In the high burnup, intermediate clad temperature section 126, a slight depletion of nickel was observed to a depth of 4.3 microns on the clad inner surface in all places investigated. In addition, many regions had a thin nickel-rich deposit on the inner cladding surface.

No evidence of reactions between uranium, plutonium, or fission products and the cladding was observed in any of the three sections examined.

IV. DISCUSSION AND CONCLUSIONS

No clad failures occurred in the elements of capsules 36B and 42B during operation in EBR-II at heating rates of ~ 30 kW/ft to calculated burnups of 3.7 and 5.0 at.%, respectively.

Fuel swelling rates were in the range from 1.5 to 2.5 vol% per at.% burnup.

Some mechanical interaction between the fuel and cladding was observed. This resulted in cladding ovality over lengths of up to 3 in.

The low fission gas release from the fuel, 6.9 to 7.7%, resulted in very low operating hoop stresses, ~ 500 psi, in the element of capsule 42B at the time of its removal from EBR-II.

Thermal stresses result in major fuel splitting on initial reactor startup and in general fragmentation as the fuel is weakened due to fission product recoil and fast neutron damage. Fuel fragmentation is more severe in the high burnup, high temperature regions of the fuel.

Bubble nucleation at grain boundaries and the depletion of beta-gamma activity in sections of fuel near the fuel centerline and the core midplane indicate that these sections operated at temperatures considerably higher than would be calculated for a solid fuel pellet. This condition could result from a decrease in the heat transfer through the fragmented fuel.

No new phases were observed in the fuel as a result of the irradiation.

The small amount of observed stainless steel carburization is probably due to carbon freed by fission and not recombined with the fission products. After long periods of time at the operating temperature, thermal effects alone cause the precipitation of carbides on the grain boundaries and twin boundaries in Type 316 stainless steel. As a result, a sigma phase (an Fe-Cr intermetallic compound) forms in the matrix austenite. This causes nickel enrichment in the austenite which can lead to formation of low melting eutectics with plutonium at the inner surface of the clad.[1] Some carburization of the clad may be beneficial in that it might suppress the loss of carbon from the austenite, thus preventing sigma phase formation.

The calculated fuel burnup was somewhat higher than the burnup determined by the ^{148}Nd method. This trend has been observed by other investigators. Burnup related quantities reported for these two experiments were referred to the calculated burnup data.

V. ACKNOWLEDGMENTS

The author is grateful to M.W. Shupe and J.A. Leary for fuel fabrication; to D.N. Dunning and L.L. Marriott for capsule loading; to J.W. Schulte, G.R. Waterbury, and K.A. Johnson for post-irradiation examination; and to J.L. Green and J.C. Clifford for fruitful discussions.

VI. REFERENCES

1. F.B. Litton and T.C. Wallace, Jr., Proceedings of Centennial Meeting of the AIME (1971).

2. J.C. Clifford, Personal Communication (February 1971).

3. M.W. Shupe, A.E. Ogard, and J.A. Leary, "Synthesis and Fabrication of Pure, Single-Phase, Uranium-Plutonium Monocarbide Pellets," LA-4283, Los Alamos Scientific Laboratory of the University of California (1970).

4. D.N. Dunning, "Loading of Sodium-Bonded Fuel Capsules," LA-4393, Los Alamos Scientific Laboratory of the University of California (1970).

5. F.A. Comprelli, S. Oldberg, and D. Sandusky, "Empirical Analysis of Swelling of Austenitic Stainless Steels in Fast Reactors," GEAP-1357, General Electric Co. (1969).

6. H.R. Brager, J.L. Straalsund, J.J. Holmes, and J.F. Bates, "Irradiation Produced Defects in Austenitic Stainless Steels," WHAN-FR-16 WADCO (1970).

7. Leslie Burris, Jr., and Ira G. Dillon, "Estimation of Fission Product Spectra in Discharged Fuel from Fast Reactors," ANL-5742, Argonne National Laboratory (1957).

8. F.L. Lisman, R.M. Abernathey, W.J. Maeck, and J.E. Rein, Nuclear Science and Engineering 42, 191 (1970).

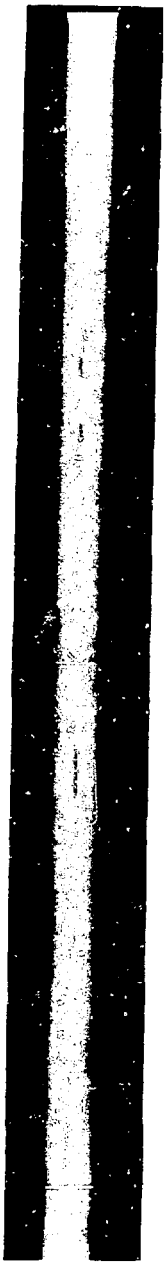

Fig. 1. Typical section from neutron radiograph of capsule 36B.

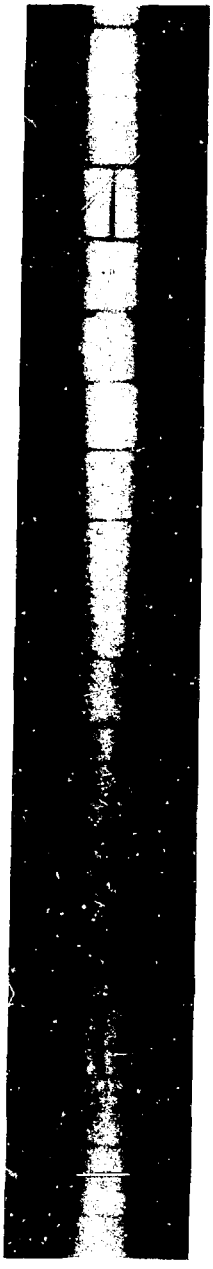

Fig. 2. Typical section from Betatron radiograph of capsule 36B. Note capped pellet.

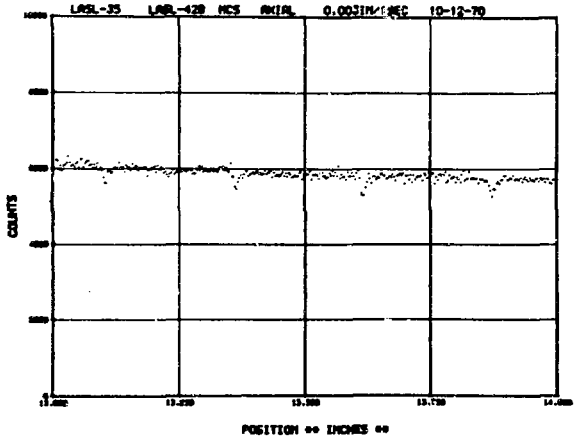

Fig. 3. Typical section from the precision gamma scan of capsule 42B. Note pellet-to-pellet interfaces.

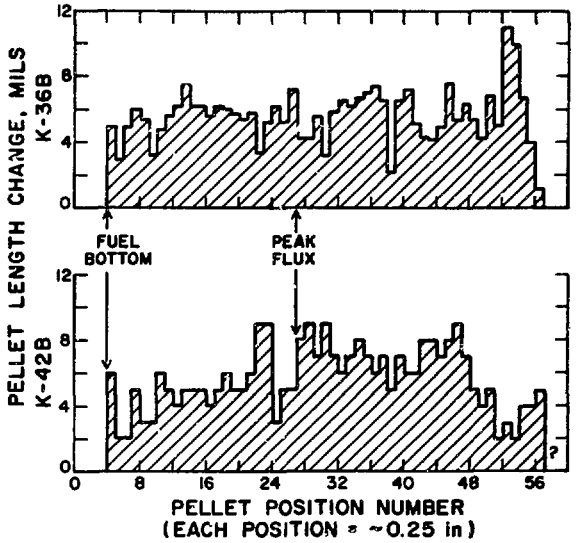

Fig. 5. Individual pellet length changes in capsules 36B and 42B as determined from precision gamma scanning.

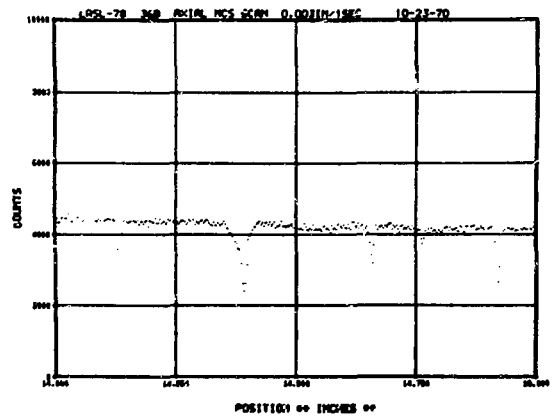

Fig. 4. Precision gamma scan of a section from capsule 36B. Note the effect of the capped pellet.

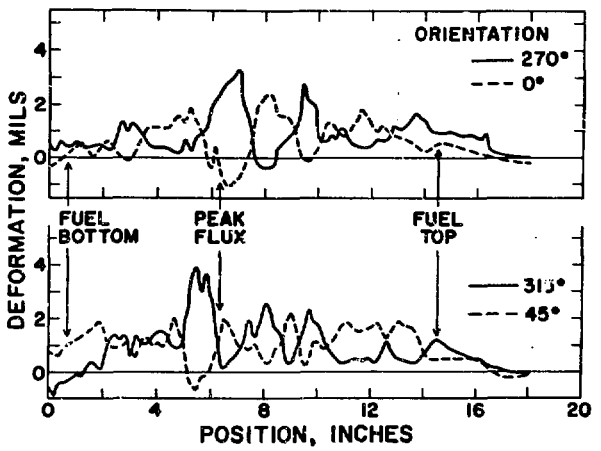

Fig. 6. Element diameter profilometry from capsule 42B.

A

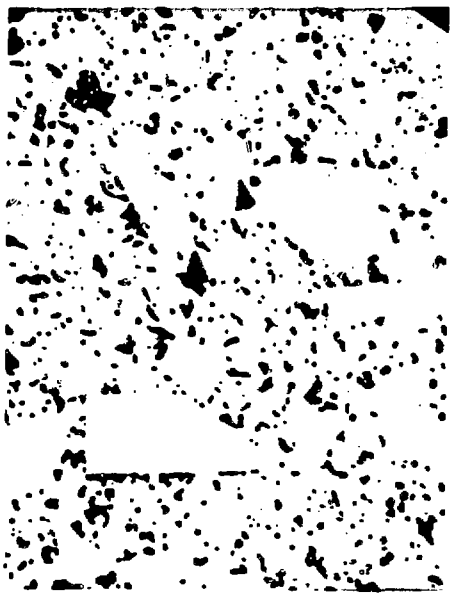

B

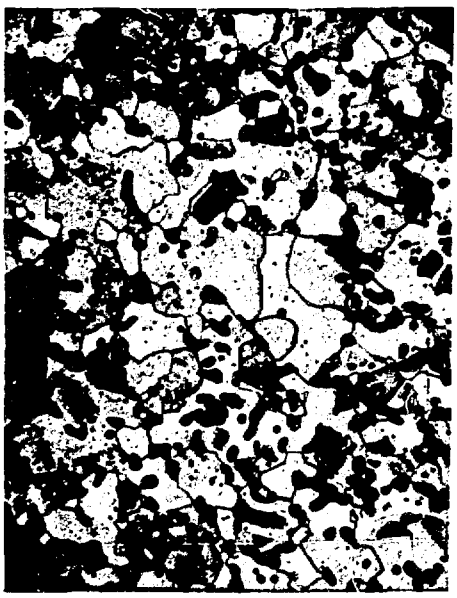

C

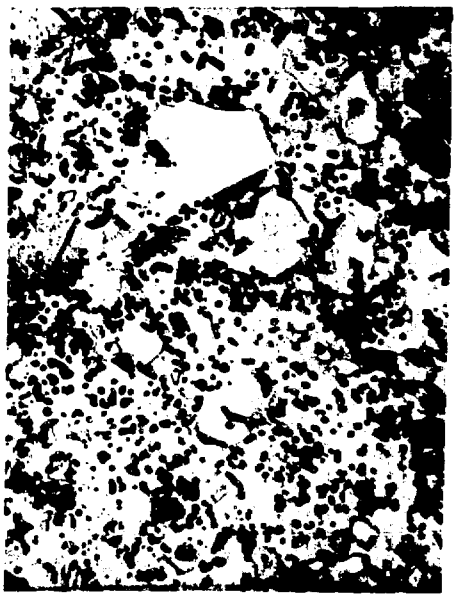

D

Fig. 7. As-polished (A and B) and etched (C and D) sections of unirradiated control fuel.

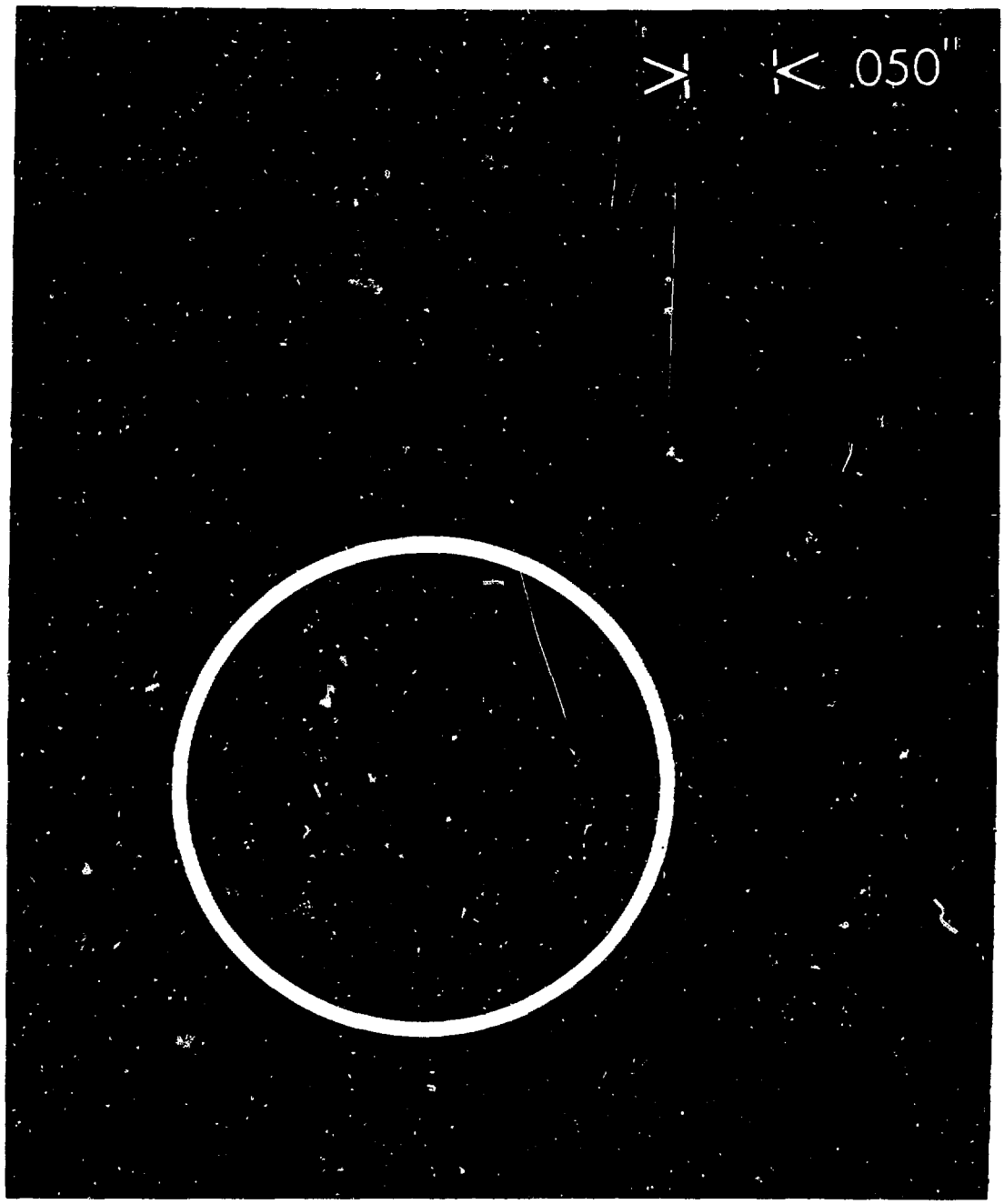

Fig. 8. As-polished macrophotograph of section 126.

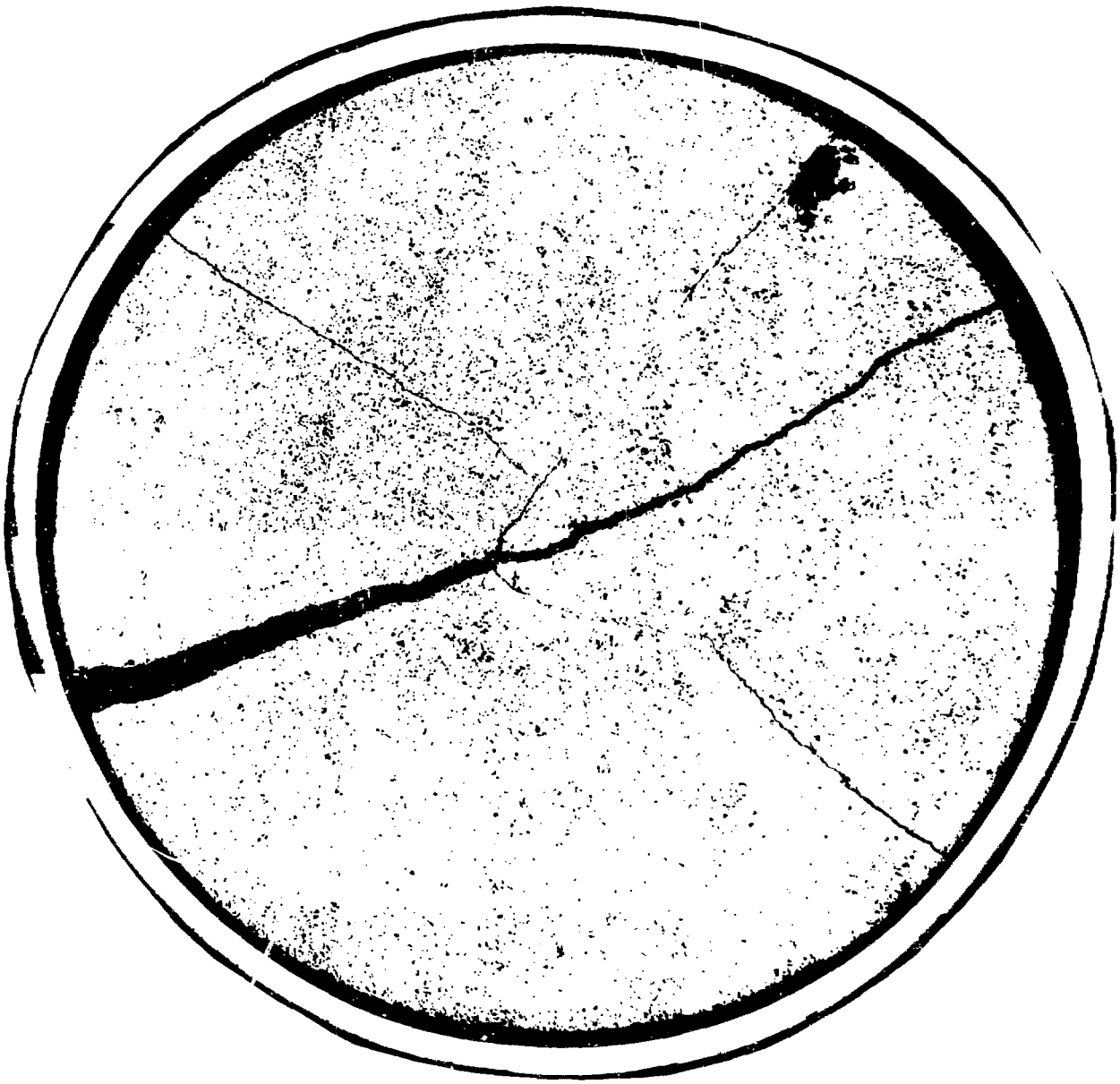

Fig. 9. As-polished mosaic of section 127.

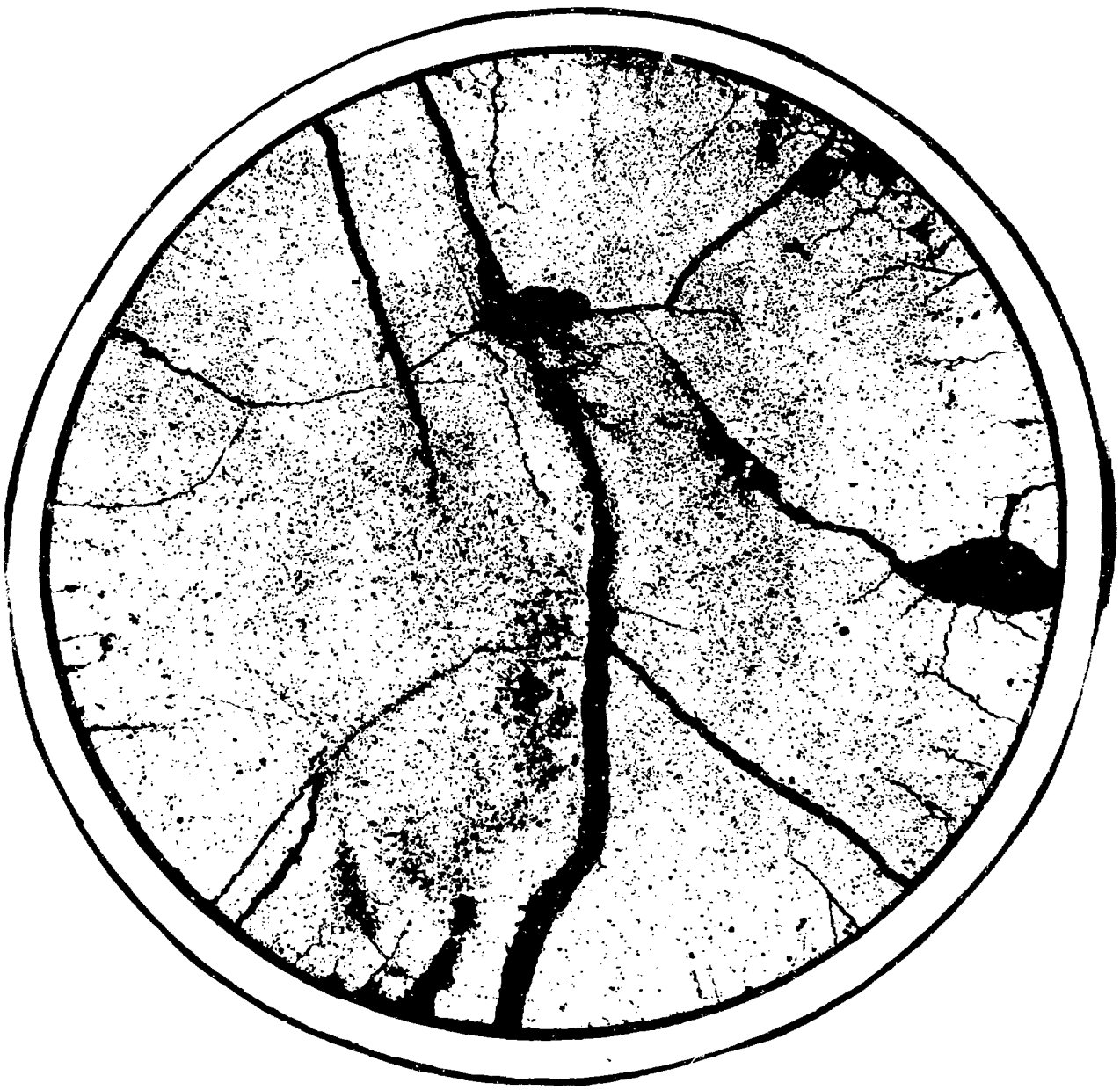

Fig. 10. As-polished mosaic of section 126.

Fig 11. As-polished mosaic of section 125.

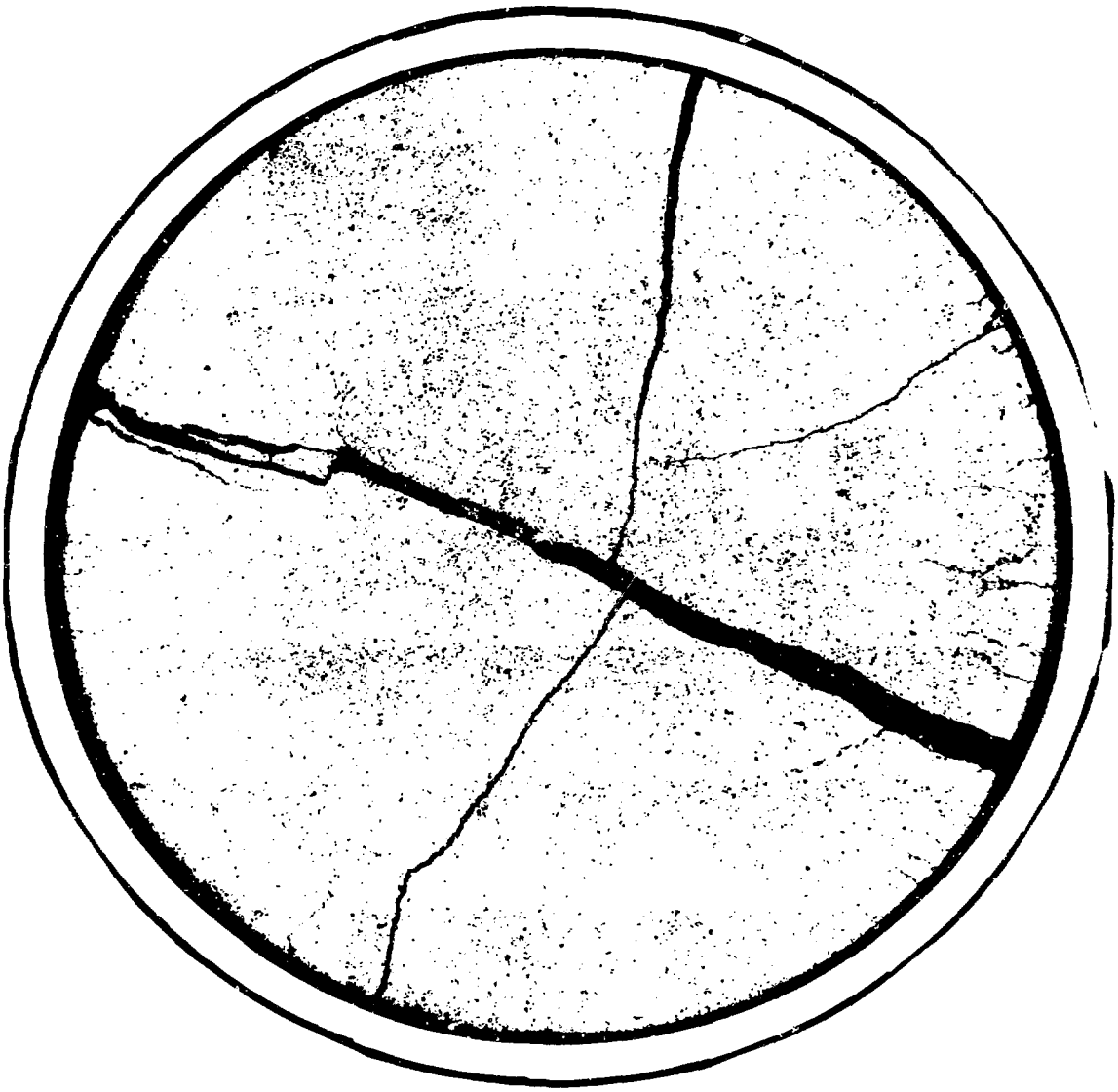

Fig. 12. As-polished mosaic of section 124.

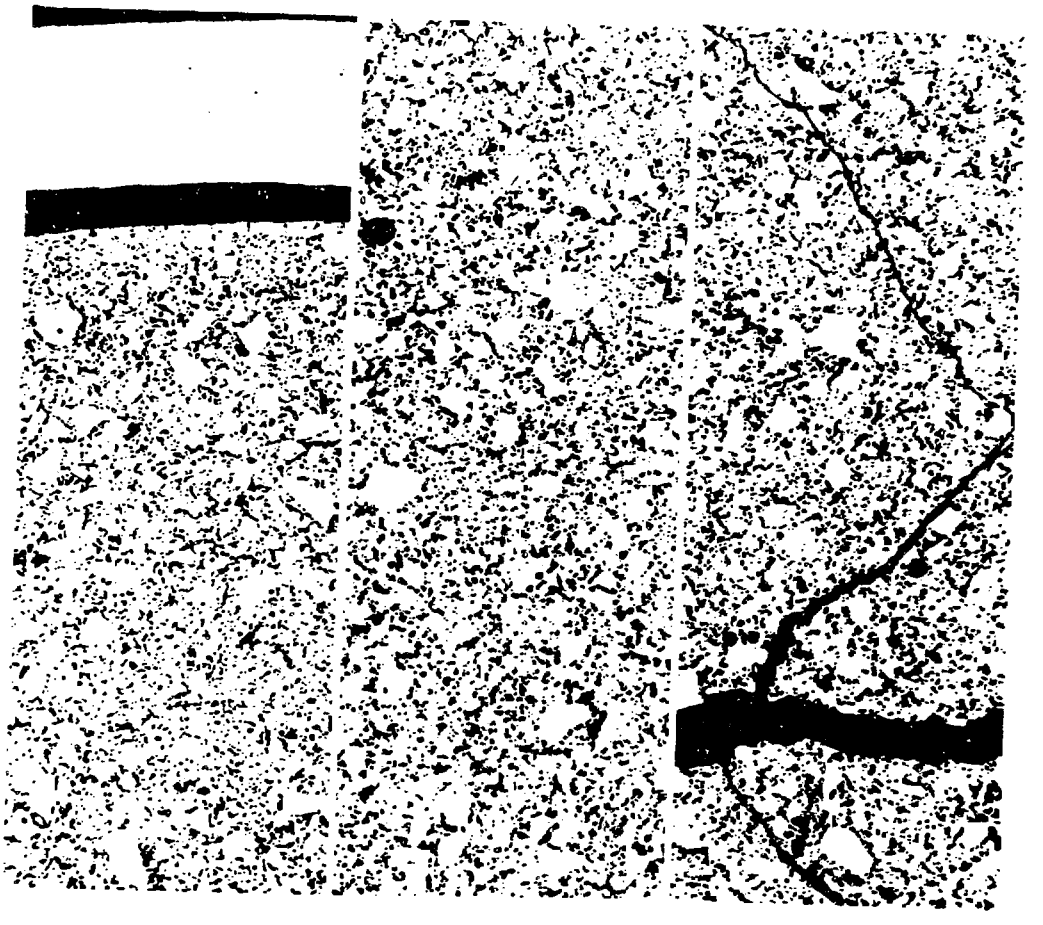

Fig. 13. As-polished radial strip of section 127.

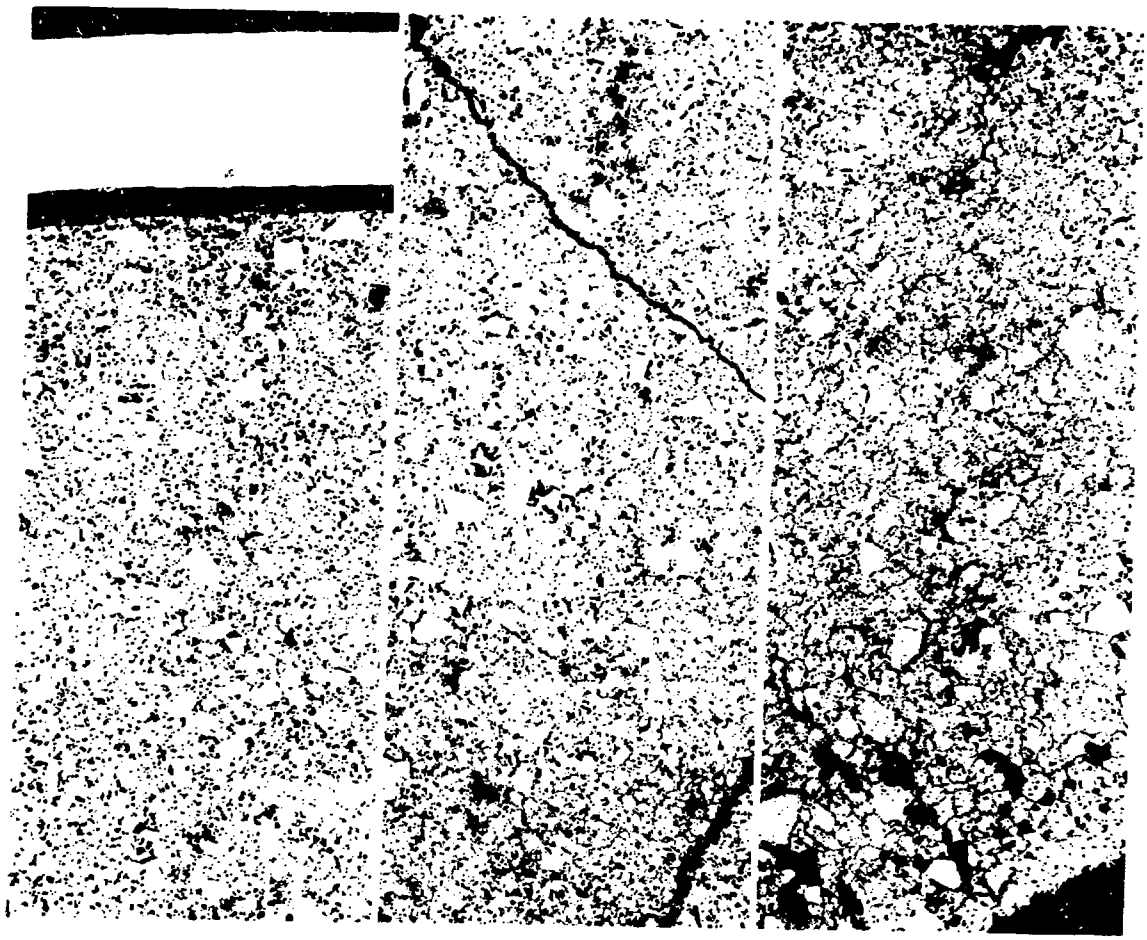

Fig. 14. As-polished radial strip of section 126.

Fig. 15. As-polished radial strip of section 125.

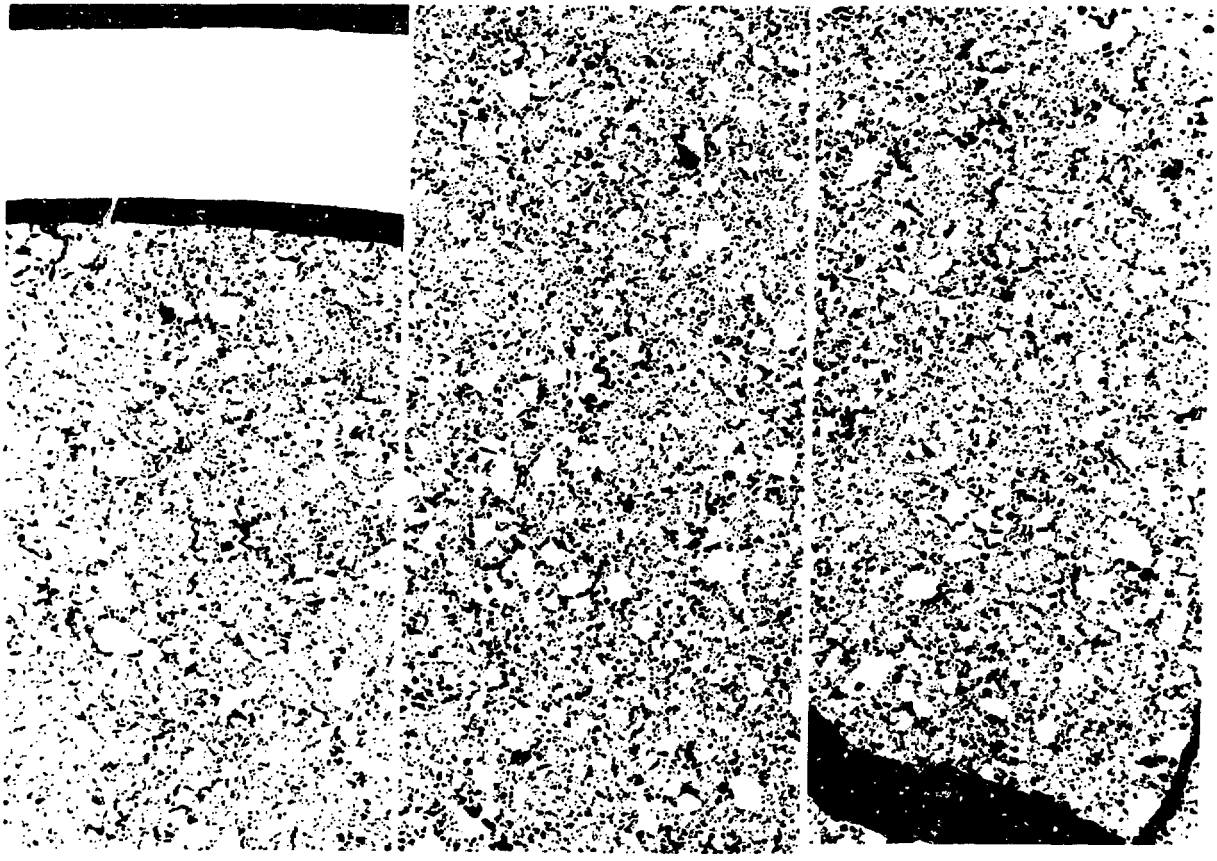

Fig. 16. As-polished radial strip of section 124.

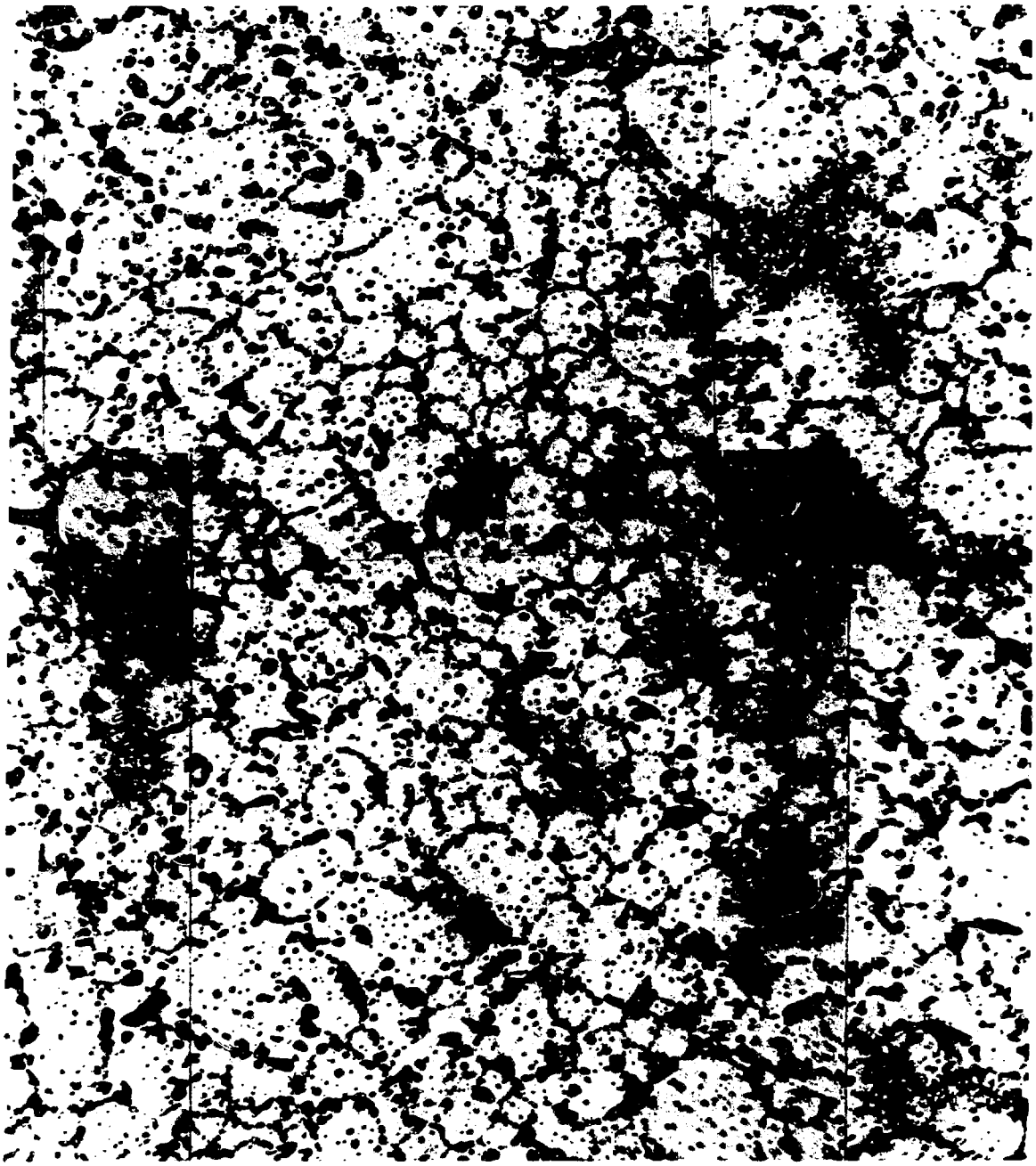

Fig. 17. As-polished section from center of section 126. Note bubble "necklaces" and stains due to weeping sodium.

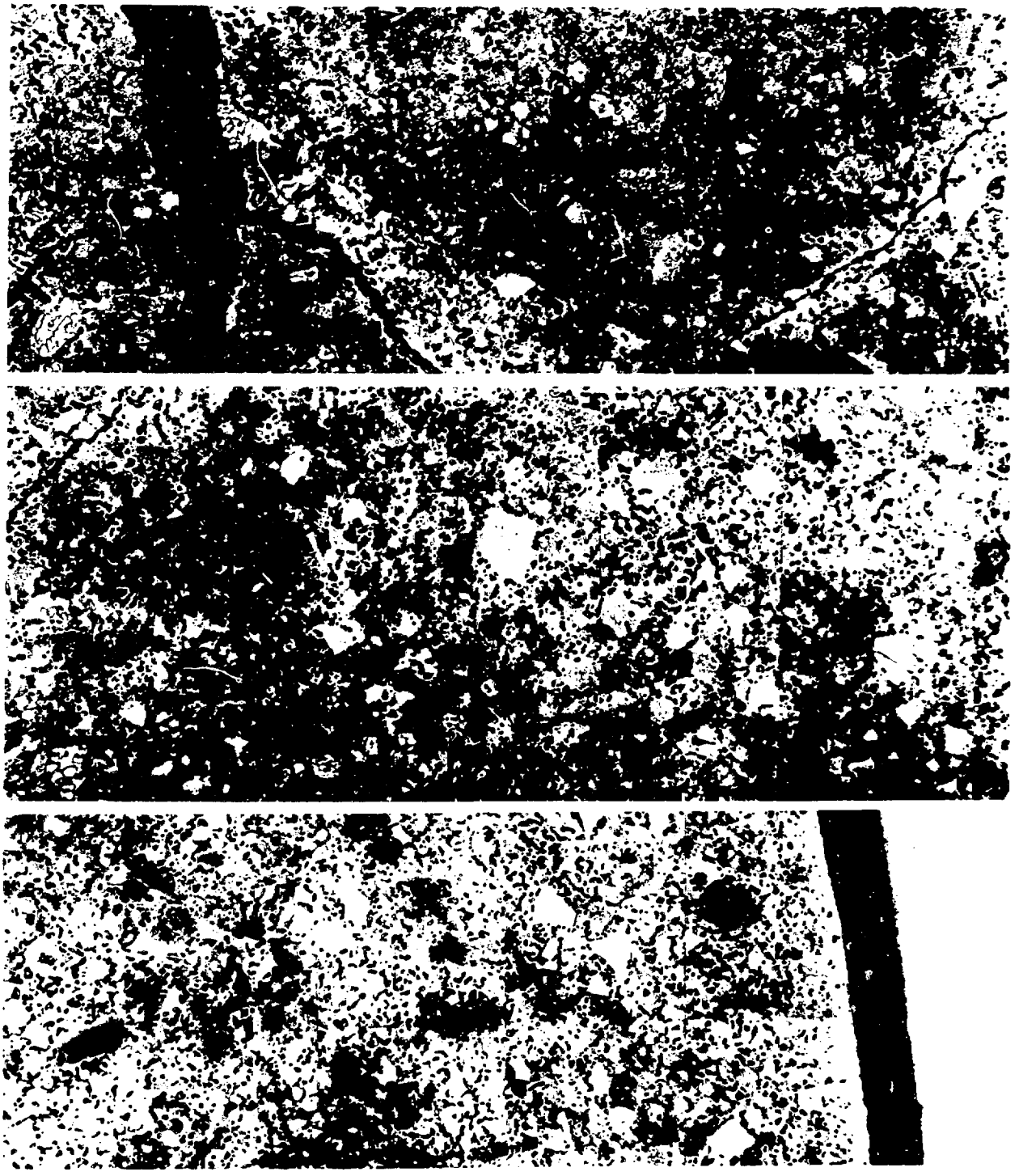

Fig. 18. Etched radial strip of fuel in section 127.

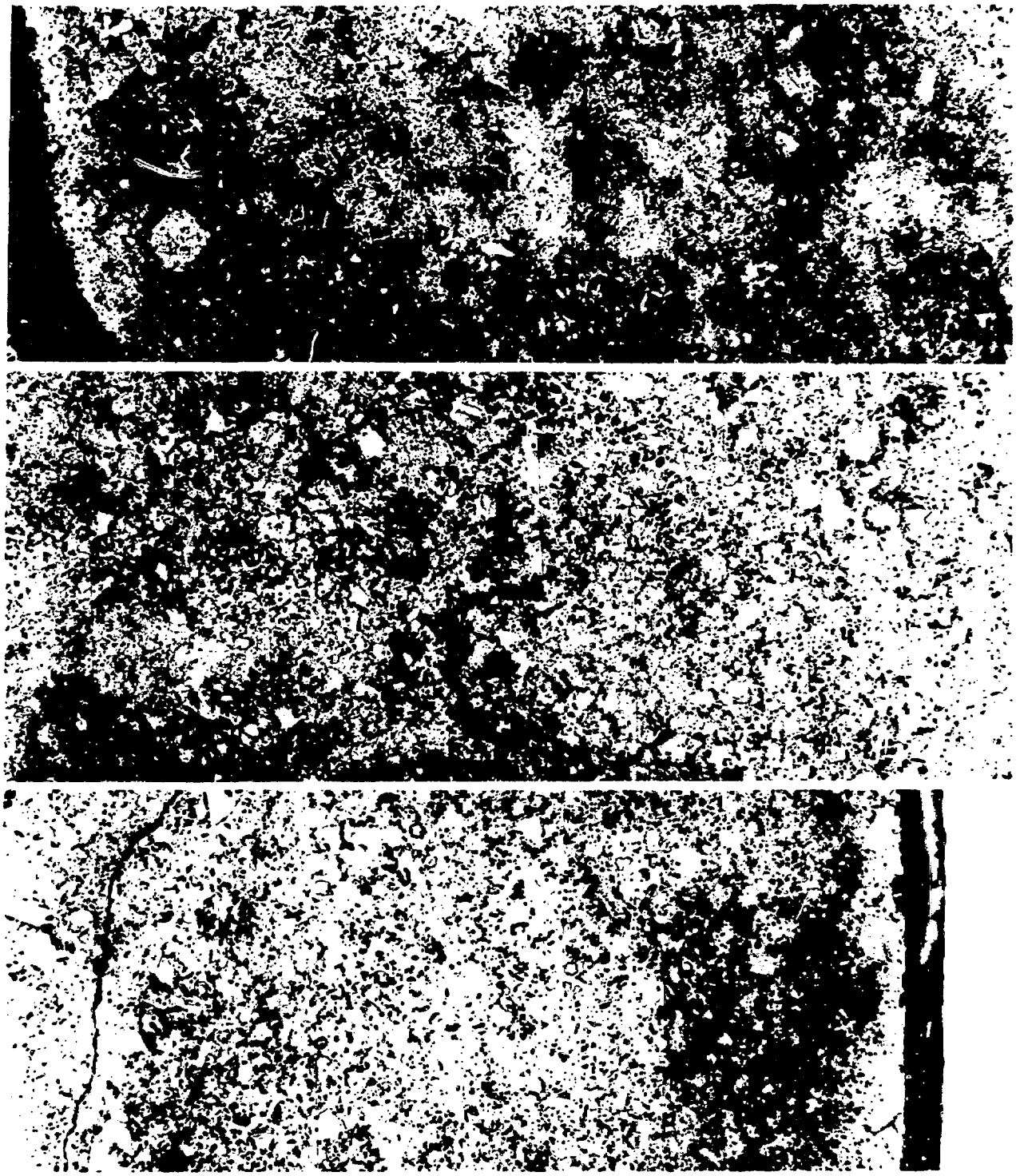

Fig. 19. Etched radial strip of fuel in section 126.

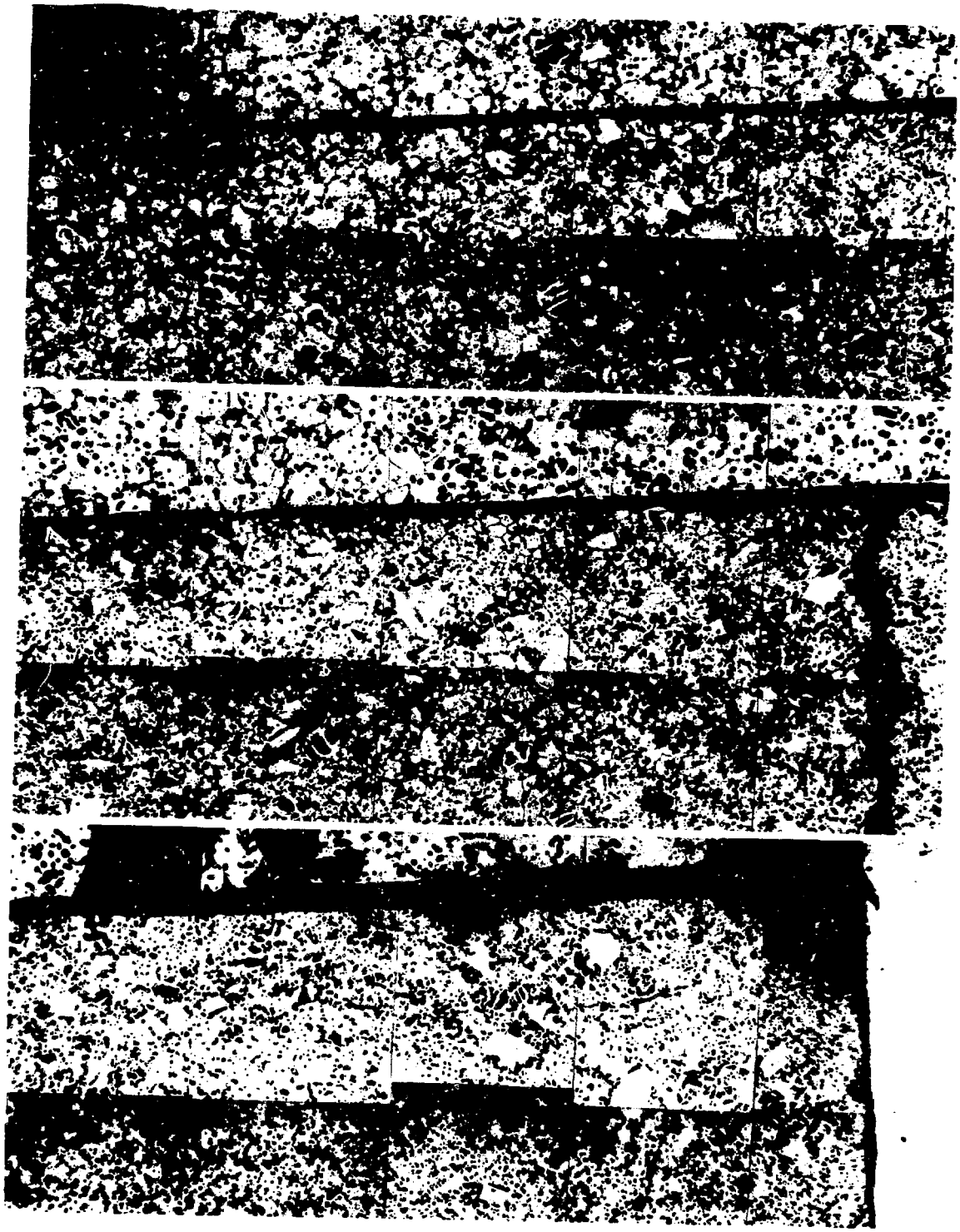

Fig. 20. Etched radial strip of fuel in section 125.

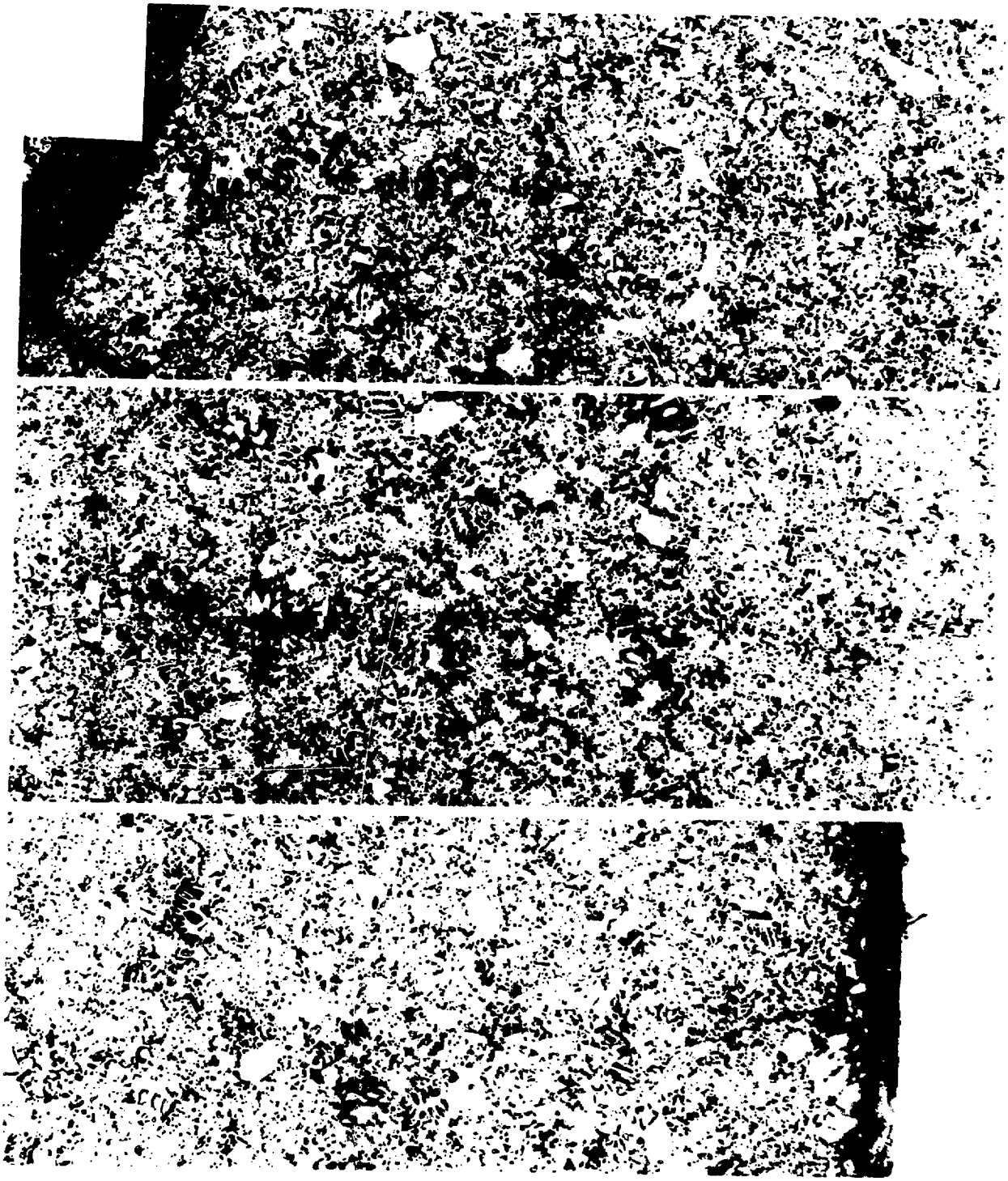

Fig. 21. Etched radial strip of fuel in section 124.

Fig. 22. Section of etched clad in section 127.

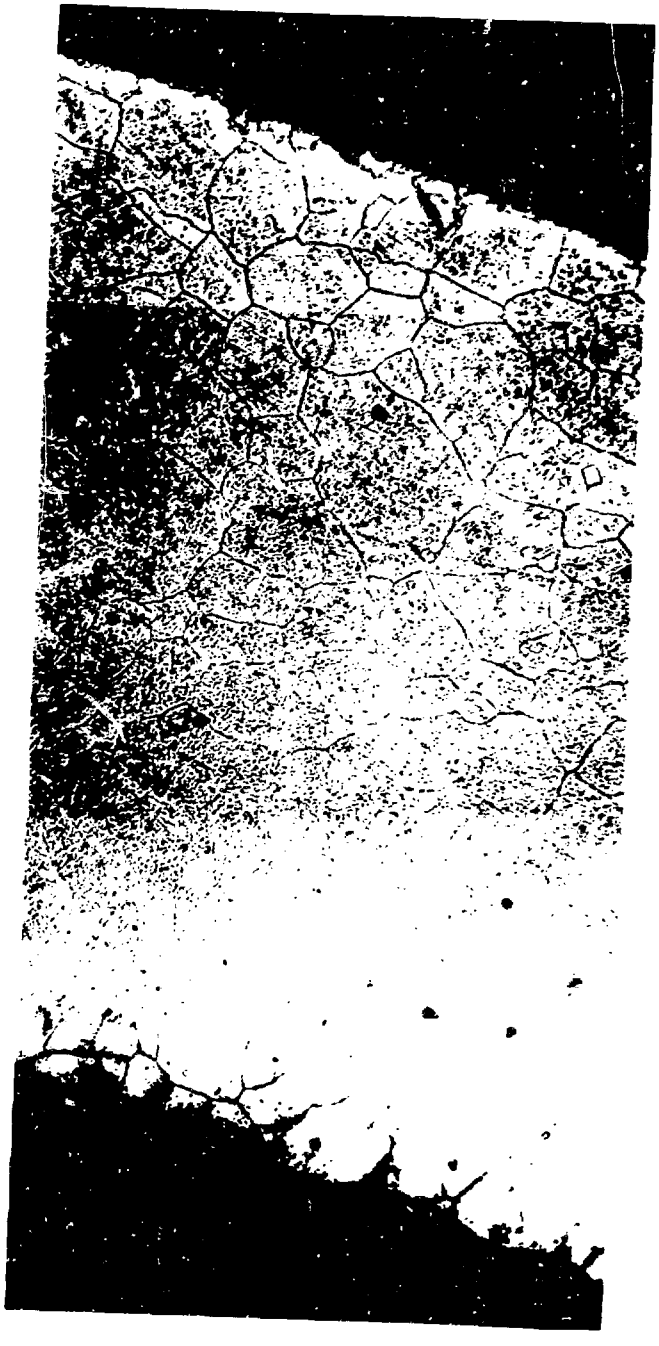

Fig. 23. Section of etched clad in section 126.

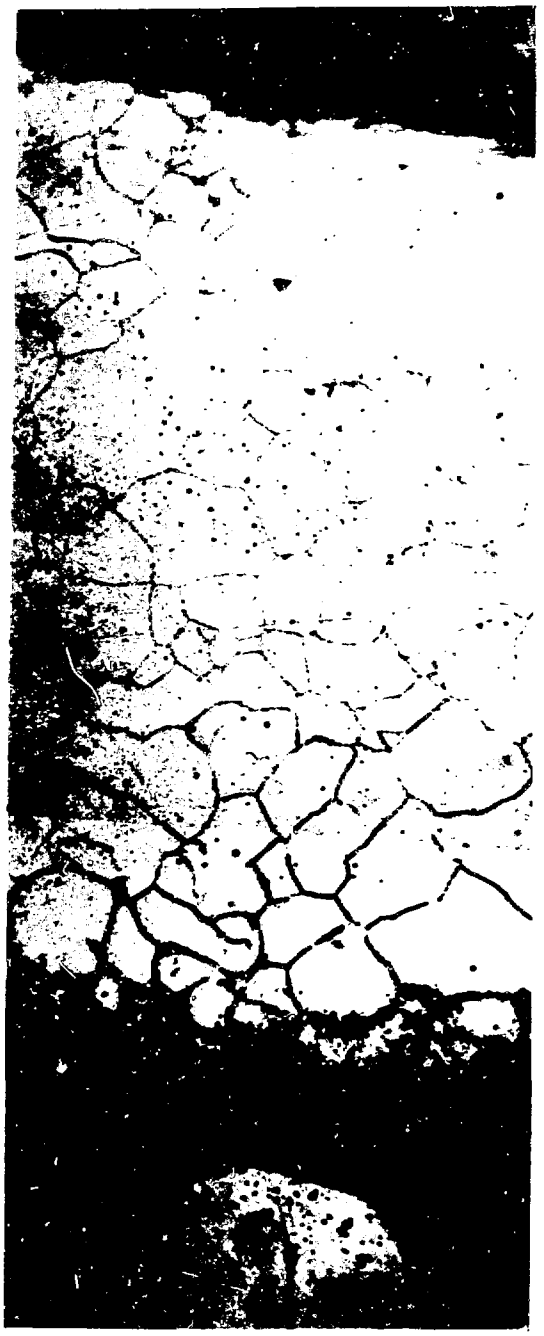

Fig. 24. Section of etched clad in section 124.

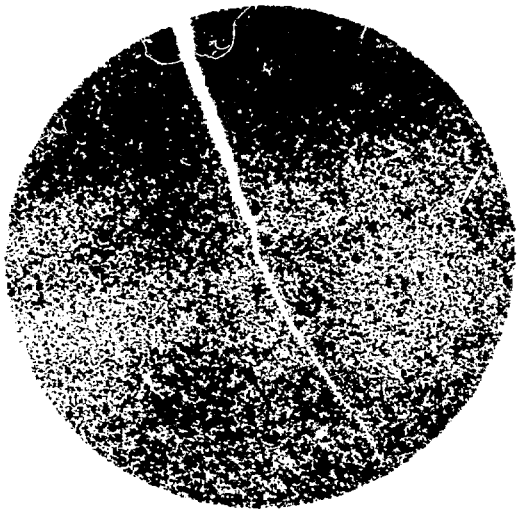

Fig. 25. Alpha autoradiograph of section 127.

Fig. 26. Alpha autoradiograph of section 126.

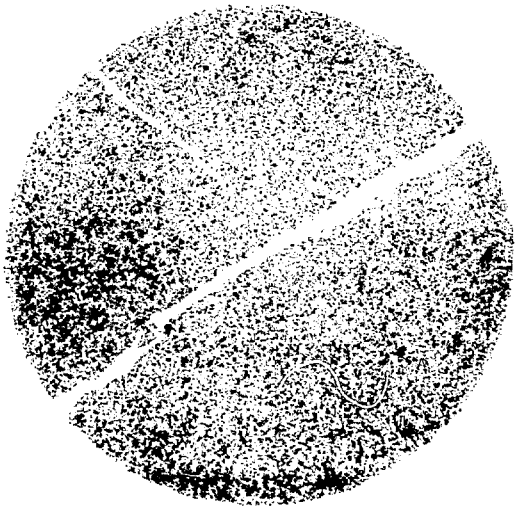

Fig. 27. Alpha autoradiograph of section 124.

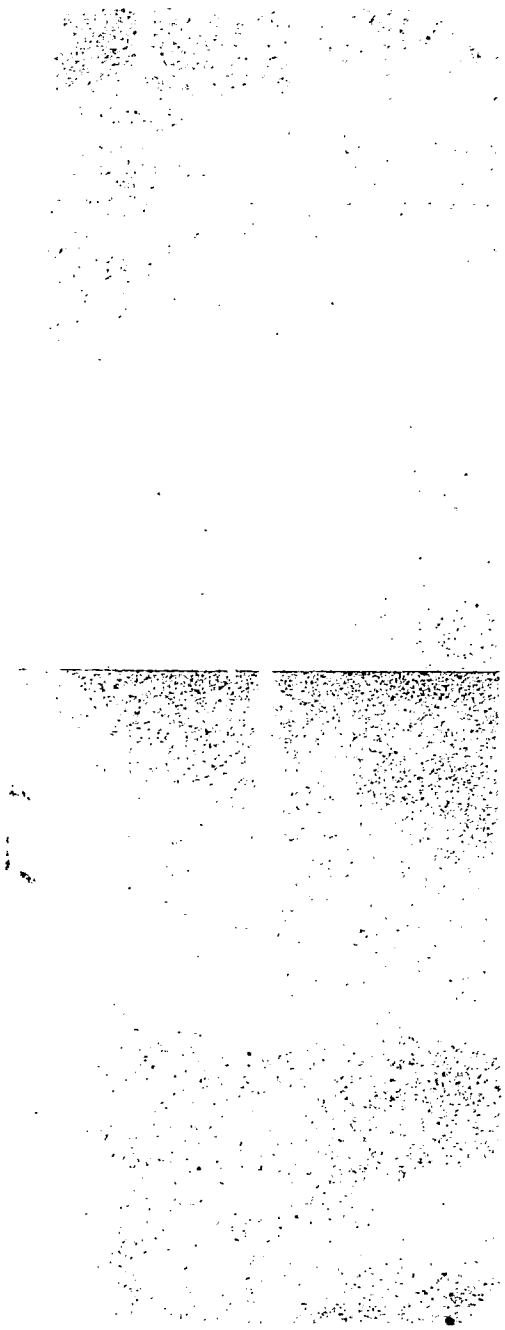

Fig. 28. Alpha autoradiograph of section 125.

Fig. 29. Beta-gamma autoradiograph of section 125.

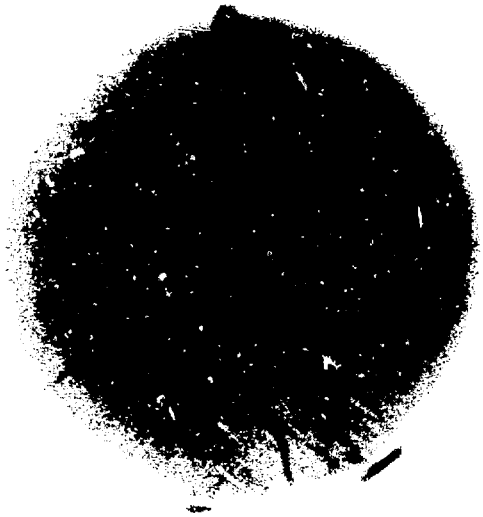

Fig. 30. Beta-gamma autoradiograph of section 127.

Fig. 31. Beta-gamma autoradiograph of section 126. Note activity depletion at center.

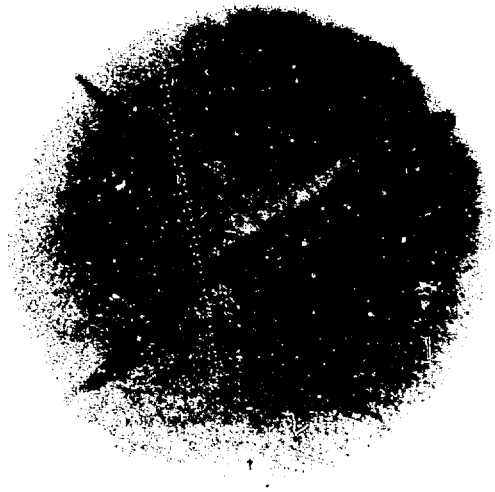

Fig. 32. Beta-gamma autoradiograph of section 124.

ALT/sp:358(100)